

Phase Retrieval by Quaternionic Reweighted Amplitude Flow on Image Reconstruction

Ren Hu^{a,b}, Pan Lian^c

^a*School of Computing and Information Technology, Great Bay University, Songshanhu international community, Songshanhu District, Dongguan, 523000, Guangdong, China*

^b*Tsinghua Shenzhen International Graduate School, Tsinghua University, Xili University Town, Nanshan District, Shenzhen, 518071, Guangdong, China*

^c*School of Mathematical Sciences, Tianjin Normal University, Binshui No.393, Xiqing District, Tianjin, 300387, Tianjin, China*

Abstract

Quaternionic signal processing provides powerful tools for efficiently managing color signals by preserving the intrinsic correlations among signal dimensions through quaternion algebra. In this paper, we address the quaternionic phase retrieval problem by systematically developing novel algorithms based on an amplitude-based model. Specifically, we propose the Quaternionic Reweighted Amplitude Flow (QRAF) algorithm, which is further enhanced by three of its variants: incremental, accelerated, and adapted QRAF algorithms. In addition, we introduce the Quaternionic Perturbed Amplitude Flow (QPAF) algorithm, which has linear convergence. Extensive numerical experiments on both synthetic data and real images, demonstrate that our proposed methods significantly improve recovery performance and computational efficiency compared to state-of-the-art approaches.

Keywords:

Phase retrieval, quaternion, color image processing, reweighted amplitude flow algorithm

1. Introduction

Over the past three decades, the use of hypercomplex numbers, such as quaternions, split quaternions, octonions, and Clifford algebras, has garnered significant attention in the representation of multidimensional signals, particularly in addressing challenges in signal and image processing, see for instance [1, 3, 6, 7]. This methodology has found

Email addresses: renhu@gbu.edu.cn (Ren Hu), pan.lian@outlook.com (Pan Lian)

wide applications in several domains, including optical imaging, array processing, wireless communications, filtering, and neural networks, see e.g., [10, 11, 12, 13, 22]. A key advantage of this approach lies in their ability of hypercomplex numbers to exploit intrinsic correlations across different signal dimensions, often resulting in compact, elegant, and interpretable frameworks for managing the geometric properties of multidimensional signals and images. This benefit arises from the algebraic structure of hypercomplex systems, which allow for both addition and multiplication, in contrast to the usual vector spaces that permit only addition and scalar multiplication. Very recently, hypercomplex techniques were applied to tackle the problem of phase retrieval in high-dimensional settings, leveraging these algebraic advantage. We refer to the recent survey [2] for the exciting new developments.

1.1. Phase retrieval and algorithm development

The original phase retrieval problem entails the reconstruction of a signal from the magnitude of its Fourier transform or the magnitude of its short-time Fourier transform, see e.g., [14, 15]. This problem has been extended to encompass general measurements. Formally,

Problem 1.1. The generalized phase retrieval problem seeks to recover a real or complex-valued signal $\mathbf{x} \in \mathbb{R}^d$ or \mathbb{C}^d from its amplitude-only measurements given by

$$b_j = |\langle \alpha_j, \mathbf{x} \rangle|, \quad j = 1, \dots, n,$$

where α_j are the measurement vectors taken from a known measurement matrix $\mathbf{A} \in \mathbb{R}^{n \times d}$ or $\mathbb{C}^{n \times d}$.

This problem arises across various scientific and engineering areas, including diffractive imaging, X-ray crystallography, astronomy, and radar waveform design [14]. Significant efforts have been dedicated to developing algorithms for conventional real and complex phase retrieval problems, which can be broadly classified into convex and non-convex approaches. While convex optimization methods (see e.g., [18, 19]) usually offer strong theoretical recovery guarantees and demonstrate strong performance, they often encounter high computational complexity in large-scale problems and may require large oversampling ratios for exact recovery. On the other hand, efficient non-convex approaches have emerged. Notably, Netrapalli et al. introduced the *AltMinPhase algorithm* in 2013 in [26]. More recently, Candès et al presented the Wirtinger Flow (WF) algorithm in their seminal work [20], which guarantees signal recovery through a simple gradient descent approach. Specifically, the WF algorithm resolves the Phase Retrieval problem via two key steps:

1. Obtaining a guess initialization using spectral method;
2. Iteratively refining this initial estimate through a gradient descent scheme to solve the intensity-based model

$$\min_{\mathbf{x} \in \mathbb{F}^d} F(\mathbf{x}) = \frac{1}{n} \sum_{j=1}^n \left(|\langle \alpha_j, \mathbf{x} \rangle|^2 - b_j^2 \right)^2, \quad (1.1)$$

where $\mathbb{F} \in \{\mathbb{R}, \mathbb{C}\}$. The success of gradient descent in WF is guaranteed by the favorable benign geometric landscape established in [31] by Sun et al. The method (WF) is further enhanced by the truncated Wirtinger flow (TWF) in [21], which employs a Poisson loss function, significantly reducing both the sample complexity to $\mathcal{O}(d)$ and the computational complexity to $\mathcal{O}(nd \log 1/\varepsilon)$.

Moreover in the real field \mathbb{R} , WF is further refined by addressing the following amplitude-based model

$$\min_{\mathbf{x} \in \mathbb{R}^d} F(\mathbf{x}) = \frac{1}{n} \sum_{j=1}^n \left(|\langle \alpha_j, \mathbf{x} \rangle| - b_j \right)^2. \quad (1.2)$$

To tackle model (1.2), Zhang et al. in [16] proposed the Reshaped Wirtinger Flow (RWF) through a simple gradient descent, while Wang et al. in [8] introduced Truncated Amplitude Flow (TAF) by truncated gradient descent; more recently Wang et al. in [17] designed Reweighted Amplitude Flow (RAF) via reweighted gradient descent. Interestingly, Zhang et al. in [16] proved that RWF enjoys the same sample complexity as TWF even without truncation in gradient steps.

Although numerical results indicate that algorithms based on the amplitude flow model (1.2) tend to outperform WF and TWF algorithms based on model (1.1) in both real and complex fields, the complex algorithms still lack rigorous theoretical guarantee. Several studies e.g., [33] have pointed out the theoretical analysis of RWF relies on the fact that the value of $\text{sign}(\langle \alpha_j, \mathbf{z} \rangle)$ equals -1 or 1 when $j = 1, \dots, n$, which can only be satisfied in the real number field. However, this condition is also essential for TWF, TAF and RAF, making straightforward generalization of theoretical results to the complex domain challenging. Some effective efforts have been made to address this problem, such as introducing new perturbed amplitude flow model [33].

Naturally, it is of interest to investigate the hypercomplex phase retrieval problem, where the signal \mathbf{x} and the entries of the measurement matrix \mathbf{A} in Prob. 1.1 take values from a specific hypercomplex algebra depending on the concrete applications. Indeed, recent interest has surged in hypercomplex phase retrieval (see, e.g., [4, 5, 9, 23]), although

it is still in its infancy. Specifically, the quaternionic phase retrieval was first considered in [23] for real-valued sensing matrix, without giving a recovery algorithm. Moreover, the model in which \mathbf{A} with real entries fails to harness the quaternion multiplication and leads to more trivial ambiguities that may limit applications of QPR. In [9], Chen and Ng considered quaternion-valued sensing matrix $\mathbf{A} \in \mathbb{H}^{m \times d}$, and introduced the quaternionic Wirtinger flow (QWF) algorithm, based on the generalized $\mathbb{H}\mathbb{R}$ calculus and the quaternion version of the intensity-based model, i.e., $\mathbb{F} = \mathbb{H}$ in model (1.1). Additionally, counterparts of TWF and TAF in QPR were proposed and demonstrating numerical improvements over QWF. These algorithms were further specialized to pure quaternion signal, effectively applied to color image recovery. Notably, the quaternionic approach achieves reconstruction with significantly fewer phaseless measurements compared to traditional real-valued phase retrieval based on monochromatic model or concatenation model. However, akin to the complex \mathbb{C} cases, QTWF and QTAF currently still lack theoretical guarantees. The octonionic phase retrieval is more challenging due to the non-associative and non-commutative structure of octonions, see [4].

1.2. Our Contribution

In this work, we consider the quaternion phase retrieval problem and systemically investigate the quaternion non-convex phase retrieval algorithms based on the quaternionic version of the amplitude-based model (1.2). Note that one key advantage of quaternionic methods is their ability to recover signals with substantially fewer measurements compared to real-valued methods based on monochromatic or concatenation models. Our algorithms are not exception. Our contributions are two fold.

(i) We introduce the Reweighted Amplitude Flow algorithm for quaternion-valued signals (QRAF), which extends the Real/Complex Amplitude Flow (RAF) algorithm originally proposed in [8]. Due to non-commutative nature of quaternion multiplication, the order of operations is crucial in our algorithm. Numerical results, presented in Section 7 show that QRAF algorithm consistently outperforms existing methods, such as QWF, QTWF and QTAF originally proposed in [9]. Notably, the Quaternionic Reshaped Wirtinger Flow (QRWF) and Quaternionic Truncated Amplitude Flow (QTAF) can be seen as special cases of QRAF. Furthermore, three variants of QRAF based on the gradient decent are introduced, which significantly enhance its performance. A detailed discussion for the convergence of QRAF is given, concluded with an open question which will be solved without significant efforts once it is solved in the complex setting.

(ii) We also introduce the Quaternionic Perturbed Amplitude Flow (QPAF). The QPAF algorithm needn't any truncation or re-weighted procedure, yet it achieves comparable numerical performance. Importantly, unlike the algorithms based on amplitude-based model (1.2), the theoretical analysis of QRAF is straightforward to extend to the present quater-

nion setting. Note that the QPAF has comparable recovery performance and computational efficiency with the QRAF.

Paper Organization and Notations The rest of this paper is organized as follows. Section 2 introduces the necessary preliminaries. In Section 3, we present the QRAF algorithm, and provide a discussion for its convergence. Section 4 explores three variants that further refine the QRAF algorithm. Section 5 focuses on the Quaternionic Perturbed Amplitude-based model and the non-convex QPAF algorithm. In Section 6, we review a useful technique—phase factor estimation—for color image processing. Experimental results on both synthetic and real-world color image data are discussed in Section 7. Concluding remarks are given in Section 8.

Throughout the paper, boldface lowercase letters such as $\alpha_i, \mathbf{x}, \mathbf{z}$ denote vectors, and boldface capital letters such as \mathbf{A}, \mathbf{Y} denote matrices. For a quaternionic matrix and a vector in \mathbb{H}^d , while \mathbf{A}^* and \mathbf{z}^* denote conjugate transposes of \mathbf{A} and \mathbf{z} , respectively. For a matrix and a vector, \mathbf{A}^T and \mathbf{z}^T denote transposes of \mathbf{A} and \mathbf{z} , respectively.

2. Preliminaries

2.1. Quaternionic Matrices

In mathematics, Hamilton’s quaternion algebra, denoted by \mathbb{H} , extends the familiar real and complex number fields. However, quaternions do not form a field because their multiplication is generally non-commutative. A quaternion $q \in \mathbb{H}$ is typically represented as

$$q = q_a + q_b i + q_c j + q_d k,$$

where $q_a, q_b, q_c, q_d \in \mathbb{R}$ and i, j, k are generalized imaginary units satisfy the relations

$$i^2 = j^2 = k^2 = -1$$

and

$$ij = -ji = k, jk = -kj = i, ki = -ik = j.$$

In this expression, the term $q_b i + q_c j + q_d k$ is called the vector part of q , while q_a is referred to as the real or scalar part. The conjugate of q is defined as $\bar{q} = q_a - q_b i - q_c j - q_d k$. For any two quaternions p and q , then $\overline{pq} = \bar{q}\bar{p}$, which is in general not equal to $\bar{p}\bar{q}$ again due to the non-commutativity of quaternion multiplication. The Euclidean norm of q is given by

$$|q| = \sqrt{q\bar{q}} = \sqrt{q_a^2 + q_b^2 + q_c^2 + q_d^2}.$$

Let \mathbb{H}^d denote the sets of d -dimensional quaternion vectors, and $\mathbb{H}^{d_1 \times d_2}$ the sets of $d_1 \times d_2$ matrices with quaternionic entries. For $\mathbf{q} = [q_k] \in \mathbb{H}^d$ and the matrix

$\mathbf{A} = [q_{ij}] \in \mathbb{H}^{d_1 \times d_2}$, the ℓ_2 norm of \mathbf{q} is defined as $\|\mathbf{q}\| = (\sum_{k=1}^d |q_k|^2)^{1/2}$ and the matrix operator norm of \mathbf{A} is given by $\|\mathbf{A}\| = \sup_{\omega \in \mathbb{H}^{d_2} \setminus \{0\}} \|\mathbf{A}\omega\|/\|\omega\|$. Let \mathbf{I}_d be the identity matrix. Similar to real and complex matrices, a matrix $\mathbf{A} \in \mathbb{H}^{d \times d}$ is called invertible if there exists a matrix \mathbf{B} such that $\mathbf{A}\mathbf{B} = \mathbf{B}\mathbf{A} = \mathbf{I}_d$. A matrix $\mathbf{A} \in \mathbb{H}^{d \times d}$ is called Hermitian if $\mathbf{A}^* = \mathbf{A}$, and unitary if $\mathbf{A}\mathbf{A}^* = \mathbf{A}^*\mathbf{A} = \mathbf{I}_d$, where \mathbf{A}^* denotes the conjugation transpose of \mathbf{A} .

The eigenvalue and eigenvector theory of a quaternion matrix is more complicated than those for real or complex matrices due to the non-commutativity. As a result, one can consider the left and right eigenvalue equations separately. In this work, we focus on the right eigenvalue and eigenvector which has its physical significance. Given $\mathbf{A} \in \mathbb{H}^{d \times d}$, if $\mathbf{A}\mathbf{x} = \mathbf{x}\lambda$ for some nonzero $\mathbf{x} \in \mathbb{H}^d$, we refer λ, \mathbf{x} as the right eigenvalue and eigenvector of \mathbf{A} . Note that $\mathbf{A}\mathbf{x} = \mathbf{x}\lambda$ is equal to $\mathbf{A}(\mathbf{x}v^*) = (\mathbf{x})v^*(v\lambda v^*)$ for any v with modulus 1. Therefore, a matrix \mathbf{A} with eigenvalue λ has a set of eigenvalues $\{v\lambda v^*\}$, from which we can select a unique ‘standard eigenvalue’ in the form of $a + bi$ with $a \in \mathbb{R}$ and $b \geq 0$). Any $\mathbf{A} \in \mathbb{H}^{d \times d}$ has exactly d standard eigenvalues, and in particular, all standard eigenvalues of Hermitian \mathbf{A} are real.

Similar to the eigenvalue decomposition for complex Hermitian matrices, a quaternion Hermitian matrix \mathbf{A} can be decomposed as $\mathbf{A} = \mathbf{U}\mathbf{\Sigma}\mathbf{U}^*$, where \mathbf{U} is a unitary matrix and $\mathbf{\Sigma}$ is diagonal, with the standard eigenvalues of \mathbf{A} arranged in the diagonal of $\mathbf{\Sigma}$. The detailed proof of the results mentioned above of quaternionic matrices can be found in [24].

2.2. Dirac Operator and Generalized HIR Calculus

In this subsection, we review the fundamentals of quaternion matrix derivatives, specifically the generalized HIR calculus introduced in [25]. This framework is essential for developing gradient-descent-like iterations in quaternionic phase retrieval algorithms. It provides a comprehensive set of rules that enable the computation of derivatives for functions directly within the quaternion domain, serving as an analogue to the Wirtinger calculus. It eliminates the need to convert the quaternionic optimization problem in (1.1) into an equivalent real-domain formulation.

For any quaternions q , consider the transformation

$$q^\mu := \mu q \mu^{-1}$$

where μ is any non-zero quaternion, which represents a 3-dimensional rotation of the vector part of q . The set $\{1, i^\mu, j^\mu, k^\mu\}$ forms a generalized orthogonal basis for \mathbb{H} . Similarly, for any quaternion vector $\mathbf{q} \in \mathbb{H}^d$, we define its transformation as $\mathbf{q}^\mu = (q_1^\mu, q_2^\mu, \dots, q_n^\mu)$.

The generalized HIR calculus can be derived either from left or right GHR derivatives. In this work, we will only use the left one. Note that in mathematical literature, the left derivative used here is often referred as the right derivative.

Definition 2.1. The left generalized $\mathbb{H}\mathbb{R}$ derivative of a function f with respect to the transformed quaternion q^μ is defined as

$$\frac{\partial_\ell f}{\partial q^\mu} = \frac{1}{4} \left(\frac{\partial f}{\partial q_a} - \frac{\partial f}{\partial q_b} i^\mu - \frac{\partial f}{\partial q_c} j^\mu - \frac{\partial f}{\partial q_d} k^\mu \right),$$

where $\partial f/\partial q_a$, $\partial f/\partial q_b$, $\partial f/\partial q_c$, and $\partial f/\partial q_d$ are the partial derivatives of f with respect to q_a , q_b , q_c , and q_d respectively.

Remark 2.2. The left and right GHR derivative operators are variants of the celebrated Dirac operators, which are widely studied in mathematical and physical literature, see e.g. [32].

Definition 2.3. For a scalar function $f(\mathbf{q})$ with $\mathbf{q} \in \mathbb{H}^n$, the gradient of f with respect to \mathbf{q} is defined as

$$\nabla_{\mathbf{q}^\mu} f = \left(\frac{\partial f}{\partial \mathbf{q}^\mu} \right)^* \in \mathbb{H}^n, \quad (2.1)$$

where $\frac{\partial f}{\partial \mathbf{q}^\mu} = \left[\frac{\partial f}{\partial q_1^\mu}, \dots, \frac{\partial f}{\partial q_n^\mu} \right]$. For simplicity, we will write $\nabla_{\mathbf{q}} f$ as ∇f in the subsequent sections.

It can be seen that $\nabla_{\mathbf{q}} f(\mathbf{q})$ represents the direction of the steepest ascent of the scalar-valued function $f(\mathbf{q})$, indicating the direction of maximum rate of change.

3. Quaternionic Reweighted Amplitude Flow

The main goal of this section is to design the Reweighted Amplitude Flow algorithm for quaternion-valued signals (QRAF), which extends the Real/Complex Amplitude Flow (RAF) algorithm originally introduced in [8]. We organize the algorithm retaining the structure of the original RAF on purpose, however, it should keep in mind that the quaternion framework introduces *non-commutativity*.

We consider the quaternionic Gaussian measurement ensemble where the entries of \mathbf{A} are i.i.d. drawn from

$$\begin{aligned} \mathcal{N}_{\mathbb{H}} := & \frac{1}{2} (\mathcal{N}(0, 1) + \mathcal{N}(0, 1)i \\ & + \mathcal{N}(0, 1)j + \mathcal{N}(0, 1)k), \end{aligned}$$

denoted by $\mathbf{A} \sim \mathcal{N}_{\mathbb{H}}^{n \times d}$, yielding $\mathbb{E}(\boldsymbol{\alpha}_k \boldsymbol{\alpha}_k^*) = \mathbf{I}_d$.

3.1. Algorithm

The QRAF algorithm is based on **the amplitude flow model**:

$$\min_{\mathbf{z} \in \mathbb{H}^d} F(\mathbf{z}) = \frac{1}{n} \sum_{j=1}^n (|\langle \alpha_j, \mathbf{z} \rangle| - \psi_j)^2,$$

where $\langle \alpha_j, \mathbf{z} \rangle = \alpha_j^* \mathbf{z}$ represents the quaternionic inner product, and $\psi_j = |\langle \alpha_j, \mathbf{x} \rangle|$ denotes the modulus of the quaternionic inner product between the known design vector α_j and the unknown solution \mathbf{x} . We assume that $\|\mathbf{x}\| = 1$.

QRAF begins with a reweighted initialization procedure, and subsequently refines the initial estimate \mathbf{z}_0 through a quaternion-based gradient descent.

3.1.1. Quaternionic Weighted Maximal Correlation Initialization

The importance of selecting an effective starting point is well-recognized for non-convex iterative algorithms in achieving the global optimum. The QRAF is not an exception.

The quaternionic weighted maximal correlation initialization consists of two steps. First, the norm of the true signal \mathbf{x} is estimated easily as:

$$\frac{1}{n} \sum_{j=1}^n \psi_j^2 = \frac{1}{n} \sum_{j=1}^n |\langle \alpha_j, \|\mathbf{x}\| \mathbf{e}_1 \rangle|^2 \approx \|\mathbf{x}\|^2. \quad (3.1)$$

Next, the direction of the quaternion signal \mathbf{x} is estimated using a flexible weighting regularization technique that balances the informative content derived from the selected data. As in the Real/Complex cases, larger ψ_i values suggest stronger a correlation between α_i and \mathbf{x} , indicating that α_i contains valuable directional information about \mathbf{x} .

More precisely, we sort the correlation coefficients $\{\psi_j\}_{1 \leq j \leq n}$ in ascending order as $0 < \psi_{[n]} \leq \dots \leq \psi_{[2]} \leq \psi_{[1]}$. Let $\mathcal{S} \subset \mathcal{M}$ denote the set of selected feature vectors α_j used for the initialization. The cardinality $|\mathcal{S}|$ is pre-defined as an integer on the order of n , e.g., $|\mathcal{S}| := \lfloor 3n/13 \rfloor$. The set \mathcal{S} is defined as the set of α_j vectors corresponding to the largest $|\mathcal{S}|$ correlation coefficients $\psi_{[j]}_{1 \leq j \leq |\mathcal{S}|}$, each approximately indicating in the direction of \mathbf{x} . It is reasonable to assume that if ψ_i is larger than ψ_j , then α_i is more correlated with \mathbf{x} than α_j is, hence providing more useful information regarding the true direction of \mathbf{x} . This motivates the assignment of higher weights to the selected α_i vectors corresponding to larger ψ_i values.

Approximating the direction of \mathbf{x} thus reduces to find a vector that maximizes its correlation with the subset \mathcal{S} of selected directional vectors α_j . The desired approximation

vector is again efficiently found by solving:

$$\begin{aligned} & \max_{\|z\|=1} \frac{1}{|\mathcal{S}|} \sum_{j \in \mathcal{S}} \omega_j^{(0)} |\langle \alpha_j, z \rangle|^2 \\ & = z^* \left(\frac{1}{|\mathcal{S}|} \sum_{j \in \mathcal{S}} \omega_j^{(0)} \alpha_j \alpha_j^* \right) z. \end{aligned}$$

Here $\omega_j^{(0)} := \psi_j^\gamma$, and γ is a carefully chosen parameter. By default, we set $\gamma = 1/2$ in the reported numerical implementations. This, combined with the norm estimate (3.1) to match the magnitude of \mathbf{x} , provides the initialization.

3.1.2. Quaternionic Adaptively Reweighted Gradient Flow

The guessed initialization vector z_0 is refined by an adaptively reweighted gradient descent. The new weighted quaternionic gradient is given by

$$\nabla \ell_{\text{rw}}(z) = \frac{1}{n} \sum_{k=1}^n \omega_k^{(t)} \left(1 - \frac{\psi_k}{|\alpha_k^* z|} \right) \alpha_k \alpha_k^* z, \quad (3.2)$$

where the adaptive weights are defined by

$$\omega_k^{(t)} = \frac{1}{1 + \beta / (|\alpha_k^* z| / |\alpha_k^* \mathbf{x}|)}, \quad 1 \leq k \leq n,$$

in which the dependence on the iterate index t is ignored for notational brevity. It should be kept in mind the multiplication order in the factor $\alpha_k \alpha_k^* z$ in (3.2) is crucial, otherwise the algorithm may fail.

The idea behind introducing this quaternionic gradient is as same as it in the conventional RAF in [8], which is to differentiate the contributions of various gradients to the overall search direction. A straightforward approach is thus to assign large weights to more reliable gradients and smaller weights to the less reliable ones. Therefore, the gradient is designed based on the ratio $|\alpha_i^* z| / |\alpha_i^* \mathbf{x}|$, which serves as a confidence score reflecting the reliability of the corresponding gradient and potentially indicating directions that lead to the true \mathbf{x} .

Taking a suitable step size η , the update rule is given by

$$z_{i+1} = z_i - \eta \cdot \nabla \ell_{\text{rw}}(z_i).$$

In summary, the QRAF algorithm, combining the initialization and gradient flow processes, is outlined in Algorithm 1.

Algorithm 1 Quaternionic Reweighted Amplitude Flow (QRAF)

Input: Data $(\alpha_k, \psi_k = |\alpha_k^* \mathbf{x}|)_{k=1}^n$, step size η , weighting parameters β , subset cardinality $|\mathcal{S}|$, exponent γ and the iteration number T ;

Output: \mathbf{z}_T ;

- 1: Let the set \mathcal{S} contains the indices of $|\mathcal{S}|$ largest entries in ψ_k , $k = 1, 2, \dots, n$.
- 2: Construct the quaternionic Hermitian matrix

$$\mathbf{S}_{in} = \frac{1}{n} \sum_{k=1}^n \omega_k^{(0)} \alpha_k \alpha_k^*,$$

where

$$\omega_k^{(0)} = \begin{cases} \psi_k^\gamma, & k \in \mathcal{S} \subset \mathcal{M}, \\ 0, & \text{otherwise,} \end{cases}$$

and find its normalized eigenvector \mathbf{v}_{in} regarding its largest standard eigenvalue.

- 3: Compute $\lambda_0 = \left(\frac{1}{n} \sum_{k=1}^n \psi_k^2\right)^{1/2}$ and obtain the spectral initialization $\mathbf{z}_0 = \lambda_0 \cdot \mathbf{v}_{in}$.
- 4: **for all** $i = 0, 1, \dots, T - 1$ **do**
- 5: Compute

$$\nabla \ell_{\text{rw}}(\mathbf{z}_i) = \frac{1}{n} \sum_{k=1}^n \omega_k^{(i)} \left(1 - \frac{\psi_k}{|\alpha_k^* \mathbf{z}_i|}\right) \alpha_k \alpha_k^* \mathbf{z}_i, \quad (3.3)$$

$$\text{where } \omega_k^{(i)} = \frac{|\alpha_k^* \mathbf{z}_i| / \psi_k}{|\alpha_k^* \mathbf{z}_i|^2 / \psi_k + \beta}.$$

- 6: Update $\mathbf{z}_{i+1} = \mathbf{z}_i - \eta \cdot \nabla \ell_{\text{rw}}(\mathbf{z}_i)$.
 - 7: **end for**
 - 8: **return** \mathbf{z}_T .
-

3.2. Linear Convergence Discussion

In this section, we present a partial analysis of the convergence of the QRAF algorithm. The primary challenge remains in establishing the local regularity condition, which is analogous to the difficulty encountered in the complex RAF algorithm, as discussed in the introduction. However, once this problem is resolved in the complex domain, we believe that extending the result to the quaternionic setting will not require significant additional effort.

We adopt the distance defined in [9] between any two vectors \mathbf{z} and \mathbf{x} in \mathbb{H}^d as follows

$$\text{dist}(\mathbf{z}, \mathbf{x}) = \min_{|w|=1} \|\mathbf{z} - \mathbf{x}w\|, \quad (3.4)$$

where $w \in \mathbb{H}$ accounts for the trivial ambiguity of the right quaternion phase factor. Recall that the minimum in the above equation (3.4) is attained at $w = \text{sign}(\mathbf{x}^* \mathbf{z})$, yielding the expression $\text{dist}(\mathbf{z}, \mathbf{x}) = \|\mathbf{z} - \mathbf{x} \text{sign}(\mathbf{x}^* \mathbf{z})\|$, where $\text{sign}(w) := w/|w|$ for nonzero $w \in \mathbb{H}$ and $\text{sign}(0) := 1$.

For the initial guess \mathbf{z}_0 , produced by the spectrum method in Algorithm 1, it is found that the weighted initialization is effective, following a similar discussion in the complex case. Hence we omit the detailed proof.

Proposition 3.1 (Weighted Initialization). For an arbitrary $\mathbf{x} \in \mathbb{H}^d$, consider the noiseless measurements $\psi_i = |\psi^* \mathbf{x}|$, $1 \leq i \leq n$. If $n \geq c_0 |S| \geq c_1 d$, then with probability exceeding $1 - c_3 e^{-c_2 n}$, the initial guess \mathbf{z}_0 obtained by the weighted maximal correlation method satisfies

$$\text{dist}(\mathbf{z}_0, \mathbf{x}) \leq \rho \|\mathbf{x}\|$$

for $\rho = 1/10$. Here $c_0, c_1, c_2, c_3 > 0$ are some absolute constants.

Next, we are expecting to prove that starting from such an initial estimate, the iterates (in Step 4 of Algorithm 1) converge at a linear rate to the global optimum \mathbf{x} . To achieve this, it suffices to show that the iterative update of QRAF is locally contractive within a relatively small neighborhood of the true signal \mathbf{x} . Thus once the initialization falls within this neighborhood, linear convergence can be ensured with an appropriate choice of the constant step size. The local error contraction, and consequently linear convergence, directly follow from the Local Regularity Condition (LRC) in a standard way.

Definition 3.2 (Local Regularity Condition). The reweighted gradient $\nabla \ell_{\text{rw}}(\mathbf{z})$ is said to satisfy the local regularity condition for positive parameters $\mu, \lambda, \varepsilon$, denoted as LRC $(\mu, \lambda, \varepsilon)$, if

$$\begin{aligned} & \text{Re} \langle \nabla \ell_{\text{rw}}(\mathbf{z}), \mathbf{z} - \mathbf{x} \phi(\mathbf{z}) \rangle \\ & \geq \frac{\lambda}{2} \text{dist}^2(\mathbf{z}, \mathbf{x}) + \frac{\mu}{2} \|\nabla \ell_{\text{rw}}(\mathbf{z})\|^2 \end{aligned}$$

holds for all $\mathbf{z} \in \mathbb{H}^d$ such that $\|\mathbf{z} - \mathbf{x} \phi(\mathbf{z})\| \leq \varepsilon \|\mathbf{x}\|$ for some constant $0 < \varepsilon < 1$. The ball given by $\|\mathbf{z} - \mathbf{x} \phi(\mathbf{z})\| \leq \varepsilon \|\mathbf{x}\|$ is termed the *basin of attraction* in literature.

Lemma 3.3 (Local error contraction). For an arbitrary $\mathbf{x} \in \mathbb{H}^d$, consider n noise-free measurements $\psi = |\alpha_j^* \mathbf{x}|$, $1 \leq j \leq n$. There exist some constants $c_1, c_2, c_3 > 0$, and $0 < \nu < 1$ such that the following holds with probability exceeding $1 - c_3 e^{-c_2 n}$

$$\text{dist}^2(\mathbf{z}_{t+1}, \mathbf{x}) \leq (1 - \nu) \text{dist}^2(\mathbf{z}, \mathbf{x})$$

for all $\mathbf{x}, \mathbf{z} \in \mathbb{H}^d$ satisfying $\text{dist}(\mathbf{z}, \mathbf{x}) \leq \frac{1}{10} \|\mathbf{x}\|$, provided that $n \geq c_1 d$ and the constant step size $\mu \leq \mu_0$, where the numerical constant μ_0 depends on the parameter $\beta > 0$ and data $\{(\alpha_i; \psi_i)\}_{1 \leq i \leq n}$.

Proof. Straightforward computations yield

$$\begin{aligned}
& \text{dist}^2(\mathbf{z} - \mu \cdot \nabla \ell_{\text{rw}}(\mathbf{z}), \mathbf{x}) \\
& \leq \|\mathbf{z} - \mu \nabla \ell_{\text{rw}}(\mathbf{z}) - \mathbf{x} \phi(\mathbf{z})\|^2 \\
& = \text{dist}^2(\mathbf{z}, \mathbf{x}) + \mu^2 \|\nabla \ell_{\text{rw}}(\mathbf{z})\|^2 \\
& \quad - 2\mu \cdot \text{Re} \langle \nabla \ell_{\text{rw}}(\mathbf{z}), \mathbf{z} - \mathbf{x} \phi(\mathbf{z}) \rangle \\
& \leq \text{dist}^2(\mathbf{z}, \mathbf{x}) + \mu^2 \|\nabla \ell_{\text{rw}}(\mathbf{z})\|^2 \\
& \quad - 2\mu \left(\frac{\mu}{2} \|\nabla \ell_{\text{rw}}(\mathbf{z})\|^2 + \frac{\lambda}{2} \text{dist}^2(\mathbf{z}, \mathbf{x}) \right) \\
& \leq (1 - \lambda\mu) \text{dist}^2(\mathbf{z}, \mathbf{x}),
\end{aligned}$$

where we used the LRC in the third step. \square

Now, the main concern reduces to prove that within the neighborhood of the global minimizer, QRAF satisfies the LRC.

Lemma 3.4. *The reweighted gradient $\nabla \ell_{\text{rw}}(\mathbf{z})$ satisfies $\text{LRC}(\mu, \lambda, \varepsilon)$.*

Proof. (I) First we show that

$$\|\nabla \ell_{\text{rw}}(\mathbf{z})\| \leq (1 + \delta) \|\mathbf{z} - \mathbf{x} \phi(\mathbf{z})\| \quad (3.5)$$

holds with high probability. As in the conventional case, rewrite the reweighted gradient in a compact matrix-vector form

$$\begin{aligned}
\nabla \ell_{\text{rw}}(\mathbf{z}) &= \frac{1}{n} \sum_{k=1}^n \omega_k^t \left(1 - \frac{y_k}{|\boldsymbol{\alpha}_k^* \mathbf{z}|} \right) \boldsymbol{\alpha}_k \boldsymbol{\alpha}_k^* \mathbf{z} \\
&= \frac{1}{n} \text{diag}(\mathbf{w}) \mathbf{A} \mathbf{v},
\end{aligned}$$

where $\text{diag}(\mathbf{w}) \in \mathbb{R}^{n \times n}$ is a diagonal matrix holding in order the entries of $\mathbf{w} = [\omega_1, \dots, \omega_n]^* \in \mathbb{R}^m$ on its main diagonal and $\mathbf{v} := [v_1, \dots, v_n]^* \in \mathbb{R}^n$ with $v_i = \left(1 - \frac{y_k}{|\boldsymbol{\alpha}_k^* \mathbf{z}|} \right) \boldsymbol{\alpha}_i^* \mathbf{z}$. It follows that

$$\begin{aligned}
\|\nabla \ell_{\text{rw}}(\mathbf{z})\| &= \left\| \frac{1}{n} \text{diag}(\mathbf{w}) \mathbf{A} \mathbf{v} \right\| \\
&\leq \frac{1}{n} \|\text{diag}(\mathbf{w})\| \cdot \|\mathbf{A}\| \cdot \|\mathbf{v}\| \\
&\leq \frac{1 + \delta_1}{\sqrt{n}} \|\mathbf{v}\|,
\end{aligned}$$

where we have used the inequalities $\|\text{diag}(\mathbf{w})\| \leq 1$ since $\omega_i \leq 1$ for all $1 \leq i \leq n$ and $\|\mathbf{A}\| \leq (1 + \delta_1)\sqrt{n}$ for some constants $\delta_1 > 0$ (see e.g., [34]), assuming that n/d is sufficiently large.

Next, we bound $\|\mathbf{v}\|$,

$$\begin{aligned} \|\mathbf{v}\|^2 &\leq \sum_{k=1}^n (|\alpha_k^* \mathbf{z}| - |\alpha_k^* \mathbf{x}|)^2 \\ &\leq \sum_{k=1}^n \|\alpha_k^* (\mathbf{z} - \mathbf{x}\phi(\mathbf{z}))\|^2 \\ &\leq (1 + \delta_2)^2 n \|\mathbf{z} - \mathbf{x}\phi(\mathbf{z})\|^2, \end{aligned}$$

for some constant $\delta_2 > 0$, which holds with probability at least $1 - e^{-c_2 n}$ as long as $n > c_1 d$.

Combining these results, and taking $\delta > 0$ larger than $(1 + \delta_1)(1 + \delta_2) - 1$, the size of $\nabla \ell_{\text{rw}}(\mathbf{z})$ can be bounded as

$$\|\nabla \ell_{\text{rw}}(\mathbf{z})\| \leq (1 + \delta) \|\mathbf{z} - \mathbf{x}\phi(\mathbf{z})\|,$$

which holds with probability $1 - e^{-c_2 n}$, with a proviso that n/d exceeds some numerical constant $c > 0$.

(II) If we can show that for all \mathbf{z} satisfying $\|\mathbf{z} - \mathbf{x}\phi(\mathbf{z})\| \leq c \|\mathbf{x}\|$, the following holds

$$\text{Re} \langle \nabla \ell_{\text{rw}}(\mathbf{z}), \mathbf{z} - \mathbf{x}\phi(\mathbf{z}) \rangle \geq c_g \|\mathbf{z} - \mathbf{x}\phi(\mathbf{z})\|^2 \quad (3.6)$$

with high probability, where $c_g > 0$ is a constant.

Combining the two bounds (3.5) and (3.6), we find that the LRC holds for μ and λ satisfying for sufficiently small ε and δ . \square

Finally, we still need to prove the following, which is open in the complex case as well. Once it is resolved in the complex setting, it will be possible to extend to the present quaternionic case without significant efforts.

Problem 3.5 (Open). If there exists a numerical constant $c > 0$ such that along the search direction $\nabla \ell_{\text{rw}}(\mathbf{z})$, the following uniform lower bound holds

$$\langle \nabla \ell_{\text{rw}}(\mathbf{z}), \mathbf{h} \rangle \geq c \|\mathbf{h}\|^2$$

for $\|\mathbf{h}\| \leq 1/10 \|\mathbf{z}\|$?

4. Further Developments of QRAF

In this section, we introduce three variants that further refine the QRAF algorithm introduced in Section 3. At the end of this section, we present the Quaternionic Reshaped Wirtinger Flow (QRWF), an extension of the RWF algorithm in [16], while the latter gives a significant improvement of the seminar work of Wirtinger Flow [20]. Notably, both the Quaternionic Truncated Amplitude Flow (QTAF) in [9] and the newly defined QRWF can be considered as special cases of the QRAF algorithm, by choosing specific weights. The efficacy of the algorithms proposed in this section will be evaluated through numerical testing.

4.1. Incremental Algorithm: QIRAF—the critical one

By reweighting the objective function at each iteration, both RAF as well as QRAF can make the gradient descent algorithm easier to converge to the global minimum. On the other side, in large-sample and online scenarios, stochastic algorithms are typically preferred due to their faster convergence rates and lower memory requirements.

In recent years, several incremental algorithms, such as Incremental Truncated Wirtinger Flow (ITWF) [27] and Incremental Reshaped Wirtinger Flow (IRWF) [16] have been developed. This further motivates the development of incremental or stochastic versions of QRAF, using mini-batches of measurements, referred to as incremental QRAF (QIRAF). The mini-batch QIRAF algorithm employs the same initialization procedure as QRAF, and use a mini-batch of measurements for each gradient update. We describe it in Algorithm 2 below. It is important to note that in [17], the mean is recommended as $\frac{1}{d}$ rather than $\frac{1}{|\Gamma|}$, which is employed in this study. Through rigorous analysis and testing, it is found that $\frac{1}{|\Gamma|}$ is a more appropriate coefficient for the quaternionic gradient of the algorithm. Additionally, the batch size of $|\Gamma| = 64$ recommended in [17] is broadly applicable; however, such value of parameter is not optimal for quaternionic cases. Here we recommended a batch size of $|\Gamma| = 2^k$, $k = \frac{\log(\frac{n}{4}-1)}{\log 2}$, which is actually the minimal value of $2^k > \frac{n}{4} - 1$.

Comparative analyses presented in Section 4 show that QIRAF exhibits good statistical and computational performance. Furthermore, QIRAF has a lower sampling complexity than QIRWF, hence provides a more efficient option in practical applications.

4.2. Accelerated Algorithm: QARAF

WF and QWF algorithms do not require manual parameter adjustment; however, their convergence rates are relatively slow. For real and complex signals, several accelerated steepest gradient methods have been proposed, demonstrating practical effectiveness (see, e.g., [29]). Convergence guarantees for these accelerated first-order methods are established in [28].

Algorithm 2 Quaternionic Mini-batch Incremental Reweighted Amplitude Flow (QIRAF)

Input: Same as in QRAF. Moreover, the size of mini-batch $|\Gamma|$;

Output: \mathbf{z}_T ;

- 1: Same spectral initialization to obtain $\mathbf{z}_0 = \lambda_0 \cdot \mathbf{v}_{in}$ as in QRAF.
- 2: **for all** $i = 0, 1, \dots, T - 1$ **do**
- 3: Uniformly select $|\Gamma|$ random number in $\{1, 2, \dots, n\}$ as the mini-batch set Γ_i and then compute

$$\nabla f(\mathbf{z}_i) = \frac{1}{|\Gamma|} \sum_{k \in \Gamma_i} \omega_k^{(i)} \left(1 - \frac{y_k}{|\boldsymbol{\alpha}_k^* \mathbf{z}_i|} \right) \boldsymbol{\alpha}_k \boldsymbol{\alpha}_k^* \mathbf{z}_i,$$

where $\omega_k^{(i)}$ is defined in (3.3).

- 4: Update $\mathbf{z}_{i+1} = \mathbf{z}_i - \eta \cdot \nabla f(\mathbf{z}_i)$.
 - 5: **end for**
 - 6: **return** \mathbf{z}_T .
-

Following the line of research, we introduce an acceleration scheme for QRAF. The initialization of \mathbf{z}_0 is selected as in the QRAF algorithm. This estimate is then refined iteratively by applying an accelerated steepest decent method to the QRAF update rule. The accelerated reweighted iterative procedure inductively is formally defined as follows,

$$\begin{cases} \mathbf{z}_{i+1} = \boldsymbol{\psi}_i - \eta \cdot \nabla f(\boldsymbol{\psi}_i), \\ \boldsymbol{\psi}_{i+1} = \mathbf{z}_{i+1} + \mu (\mathbf{z}_{i+1} - \mathbf{z}_i), \end{cases} \quad (4.1)$$

where $i = 1, 2, \dots, T$, $\eta > 0$ is the step size which is suggested as $\eta = 6$, and $\boldsymbol{\psi}_0 = \mathbf{z}_0$. This algorithm is termed as Quaternionic Accelerated Reweighted Flow (QARAF) when the extrapolation parameter $\mu = 0.8$ in Equ. (4.1) is chosen as suggested by Nesterov's method. The QARAF algorithm is presented in Algorithm 3. Comparative analyses in Fig. 1 and 2 show that QARAF converges significantly faster than QWF, QTAF, QRWF and QRAF. Fig. 3 shows that QARAF also has better performance on the success rates than QWF, QTAF and QRAF.

4.3. Adapted Algorithm: QAdRAF

In this subsection, we adopt another steepest gradient scheme, i.e. the adapted gradient decent method, in the updated rule of the QRAF algorithm, referred to as Quaternion Adaptive Reweighted Amplitude Flow (QAdRAF). As one can see in Fig. 1 and 2, it preforms the second fast convergence rate among those quaternion algorithms. QAdRAF also has nice success rate performance, see Fig. 4. This algorithm is detailed in Algorithm 4.

Algorithm 3 Quaternionic Accelerated Reweighted Amplitude Flow (QARAF)

Input: Same as in QRAF. Moreover, set the accelerator parameter μ .

Output: \mathbf{z}_T ;

- 1: Same spectral initialization to obtain $\mathbf{z}_0 = \lambda_0 \cdot \mathbf{v}_{in}$ as in QRAF.
- 2: **for all** $i = 0, 1, \dots, T - 1$ **do**
- 3: Compute $\nabla f(\mathbf{z}_i)$ as in QRAF in (3.3).
- 4: Let $\boldsymbol{\psi}_0 = \mathbf{z}_0$, then update

$$\begin{cases} \mathbf{z}_{i+1} = \boldsymbol{\psi}_i - \eta \cdot \nabla f(\boldsymbol{\psi}_i), \\ \boldsymbol{\psi}_{i+1} = \mathbf{z}_{i+1} + \mu (\mathbf{z}_{i+1} - \mathbf{z}_i). \end{cases}$$

5: **end for**

6: **return** \mathbf{z}_T .

Algorithm 4 Quaternionic Adaptive Reweighted Amplitude Flow (QAdRAF)

Input: Same as in QRAF. Moreover, set the coefficient $\mu \in (0, 1)$ and parameter ϵ ;

Output: \mathbf{z}_T ;

- 1: Same spectral initialization to obtain $\mathbf{z}_0 = \lambda_0 \cdot \mathbf{v}_{in}$ as in QRAF.
- 2: **for all** $i = 0, 1, \dots, T - 1$ **do**
- 3: Compute $\nabla f(\mathbf{z}_i)$ as in QRAF in (3.3).
- 4: Let $S_0 = 0$ and $S_{i+1} = \mu S_i + (1 - \mu) |\nabla f(\mathbf{z}_i)|^2$, then we compute

$$\eta = \frac{\alpha}{(S_{i+1} + \epsilon)^{1/2}},$$

5: Update $\mathbf{z}_{i+1} = \mathbf{z}_i - \eta \cdot \nabla f(\mathbf{z}_i)$.

6: **end for**

7: **return** \mathbf{z}_T .

4.4. QRWF Algorithm

The Reshaped Wirtinger Flow (RWF), as introduced in [16], represents a significant extension of the seminal work of Wirtinger Flow in [20]. It has nice performance but without complicated truncated procedure as TAF in [8]. Here, we introduce the Quaternionic Reshaped Wirtinger Flow (QRWF) in analogy. The QRWF can be viewed as a special case of the QRAF by selecting an appropriate weight, which is summarized in Algorithm 5.

Algorithm 5 Quaternionic Reshaped Wirtinger Flow (QRWF)

Input: $(\alpha_k, y_k = |\alpha_k^* x|)_{k=1}^n$, set step size η , lower and upper thresholds α_ℓ and α_u and iteration number T ;

Output: z_T ;

- 1: Compute $\lambda_0 = \frac{nd}{\sum_{k=1}^n \|\alpha_k\|_1} \left(\frac{1}{n} \sum_{k=1}^n y_k \right)$.
- 2: Construct the data matrix

$$\mathbf{S}_{in} = \frac{1}{n} \sum_{k=1}^n y_k \alpha_k \alpha_k^* \mathbf{1}_{\{\alpha_\ell \lambda_0 < y_k < \alpha_u \lambda_0\}},$$

where

$$\mathbf{1}_{\{\alpha_\ell \lambda_0 < y_k < \alpha_u \lambda_0\}} = \begin{cases} 1, & \alpha_\ell \lambda_0 < y_k < \alpha_u \lambda_0, \\ 0, & \text{otherwise,} \end{cases}$$

and find the normalized eigenvector \mathbf{v}_{in} of \mathbf{S}_{in} regarding its largest standard eigenvalue.

- 3: The spectral initialization can be obtained as $\mathbf{z}_0 = \lambda_0 \cdot \mathbf{v}_{in}$.
- 4: **for all** $i = 0, 1, \dots, T - 1$ **do**
- 5: Compute

$$\nabla f(\mathbf{z}_i) = \frac{1}{n} \sum_{k=1}^n \left(1 - \frac{y_k}{|\alpha_k^* \mathbf{z}_i|} \right) \alpha_k \alpha_k^* \mathbf{z}_i,$$

- 6: Update $\mathbf{z}_{i+1} = \mathbf{z}_i - \eta \cdot \nabla f(\mathbf{z}_i)$.
 - 7: **end for**
 - 8: **return** \mathbf{z}_T .
-

5. Quaternionic Perturbed Amplitude Flow (QPAF)

The TAF, TWF, and RAF algorithms for complex signals, as previously discussed, lack a comprehensive theoretical analysis. To address this issue, a new model was introduced in [33], defined as

$$\min_{\mathbf{z}} f_{\boldsymbol{\varepsilon}}(\mathbf{z}) = \min_{\mathbf{z}} \frac{1}{n} \sum_{j=1}^n \left(\sqrt{|\alpha_j^* \mathbf{z}|^2 + \varepsilon_j^2} - \sqrt{b_j^2 + \varepsilon_j^2} \right)^2, \quad (5.1)$$

where $\boldsymbol{\varepsilon} = [\varepsilon_1, \dots, \varepsilon_n] \in \mathbb{R}^n$ is a vector with prescribed values, subject to the condition that $\varepsilon_j \neq 0$ for all $b_j \neq 0$. When $\varepsilon_j = 0$ for all $j = 1, \dots, n$, this model reduces to

the amplitude-based model (1.2), and is therefore referred to as the perturbed amplitude-based model. Based on this formulation, a new non-convex algorithm, called the perturbed Amplitude Flow (PAF) is developed. The PAF algorithm can recover the target signal under $O(d)$ Gaussian random measurements. Starting from a well-designed initial point, PAF converges at a linear rate for both real and complex signals, without requiring truncation or reweighted procedures, while maintaining strong empirical performance.

In this section, we extend this framework to the Quaternionic Perturbed Amplitude Flow (QPAF) algorithm, of course utilizing the generalized $\mathbb{H}\mathbb{R}$ calculus. Numerical experiments show that QPAF performs comparably to PRAF, and significantly outperforms QTWF and QWF (see Section 4). Crucially, the primary advantage of the model (5.1) is preserved when generalized to the quaternionic setting. Specifically, with an appropriate choice of ε , the gradient $\nabla f_\varepsilon(\mathbf{z}_i)$ can be effectively controlled in the neighbourhood of the initial guess. Moreover, the gradient $\nabla f_\varepsilon(\mathbf{z}_i)$ satisfies $\text{LRC}(\mu, \lambda, \varepsilon)$, addressing the primary theoretical limitation of QRAF, see Problem 3.5. Consequently, QPAF has a linear convergence rate. Since the proof closely mirrors the original, except with special attention given to the order of quaternion multiplication, the full details are omitted here for brevity. The QPAF algorithm is provided in the following Algorithm 6.

6. Algorithm regarding to RGB picture

In quaternion image processing, the color channels (Red, Green, and Blue channels) are usually represented by the three imaginary components of quaternions, making the desired signal taking pure quaternions. Many studies (see e.g., [35]) opt to eliminate the real part of the quaternion signals after reconstruction. However, this approach generally performs poorly in the context of phase retrieval for pure quaternion signals. A more effective approach is to incorporate the pure quaternion assumption directly into the recovery process, as done in [9]. In this section, we brief review of the Phase Factor Estimate (QPFE) technique used in [9], which will be applied to refine our algorithms introduced in previous sections and then applied to phase retrieval of natural images.

Recall that for a quaternion number $q = q_0 + q_1i + q_2j + q_3k$, we call $\mathcal{R}(q) = q_0$ the real part of q and $\mathcal{P}^\theta(q)$, $\theta = i, j, k$ as the imaginary parts of q , i.e. $\mathcal{P}^i(q) = q_1$, $\mathcal{P}^j(q) = q_2$ and $\mathcal{P}^k(q) = q_3$. Let \mathbf{q} be a quaternion signal in \mathbb{H}^d , the projection \mathcal{V} splits this vector to its real and imaginary parts, i.e. $\mathcal{V}(\mathbf{q}) = [\mathcal{R}(\mathbf{q}), \mathcal{P}^i(\mathbf{q}), \mathcal{P}^j(\mathbf{q}), \mathcal{P}^k(\mathbf{q})] \in \mathbb{R}^{d \times 4}$. Furthermore, when $q_0 = 0$, the quaternion number $q = q_1i + q_2j + q_3k$ is called by pure quaternion. Then, for a pure quaternion signal $\mathbf{p} \in \mathbb{H}^d$, we have $\mathcal{V}(\mathbf{p}) = [0, \mathcal{P}^i(\mathbf{p}), \mathcal{P}^j(\mathbf{p}), \mathcal{P}^k(\mathbf{p})] \in \mathbb{R}^{d \times 4}$.

The Phase Factor Estimate is not a complete algorithm for Phase retrieval but rather a simple yet useful technique that transforms a full quaternion signal to a pure quaternion with minimal difference. The strategy of QPFE is to find a quaternion phase factor q with

Algorithm 6 Quaternionic Perturbed Amplitude Flow (QPAF)

Input: Data $(\alpha_k, \psi_k = |\alpha_k^* \mathbf{x}|)_{k=1}^n$, step size η , weighting parameter γ , the control coefficient σ and the iteration number T ;

Output: \mathbf{z}_T ;

- 1: Compute $\lambda_0 = \left(\frac{1}{n} \sum_{k=1}^n \psi_k^2\right)^{1/2}$.
- 2: Construct the quaternionic Hermitian matrix

$$\mathbf{S}_{in} = \frac{1}{n} \sum_{k=1}^n \left(\gamma - e^{-\psi_k^2/\lambda_0^2}\right) \alpha_k \alpha_k^*,$$

and find its normalized eigenvector \mathbf{v}_{in} regarding its largest standard eigenvalue.

- 3: The initialization $\mathbf{z}_0 = \lambda_0 \cdot \mathbf{v}_{in}$.
- 4: **for all** $i = 0, 1, \dots, T - 1$ **do**
- 5: Compute

$$\nabla f_{\boldsymbol{\varepsilon}}(\mathbf{z}_i) = \frac{1}{n} \sum_{k=1}^n \left(1 - \frac{\sqrt{\psi_k^2 + \boldsymbol{\varepsilon}_k^2}}{\sqrt{|\alpha_k^* \mathbf{z}_i|^2 + \boldsymbol{\varepsilon}_k^2}}\right) \alpha_k \alpha_k^* \mathbf{z}_i, \quad (5.2)$$

where $\boldsymbol{\varepsilon} = \sqrt{\sigma} \boldsymbol{\psi}$, in which $\boldsymbol{\psi} = \{\psi_k\}$, $k = 1, 2, \dots, n$.

- 6: Update $\mathbf{z}_{i+1} = \mathbf{z}_i - \eta \cdot \nabla f_{\boldsymbol{\varepsilon}}(\mathbf{z}_i)$.
 - 7: **end for**
 - 8: **return** \mathbf{z}_T .
-

$\|q\| = 1$ such that $\mathbf{z}q$ is closest to pure quaternion signal, i.e.,

$$\hat{q} = \arg \min_{\|q\|=1} \|\operatorname{Re}(\mathbf{z}q)\| \quad (6.1)$$

and then we map \mathbf{z} to the imaginary part of $\mathbf{z}\hat{q}$. The above optimization problem (6.1) can be easily solved by spectrum method after transformed to an equivalent real matrix. The detailed process is summarized in Algorithm 7. It is important to note that in Algorithm 3 in [9], the $q_{(i+1)T_p}$ should be its quaternion conjugate $\overline{q_{(i+1)T_p}}$.

Under suitable conditions, the pure quaternion signals can be exactly recovered as shown in [9]. Thus, in this case, it is more natural to adopt the distance $\operatorname{dist}_p(\boldsymbol{\omega}, \mathbf{z})$ to measure the reconstruction error of pure quaternion signals, defined as

$$\operatorname{dist}_p(\boldsymbol{\omega}, \mathbf{z}) = \min \{\|\mathbf{z} + \boldsymbol{\omega}\|, \|\mathbf{z} - \boldsymbol{\omega}\|\}. \quad (6.2)$$

In the following experiments, we always use this distance to measure the pure quaternion signal unless stated otherwise.

Algorithm 7 Quaternionic Phase Factor Estimate (QPFE)

Input: An array $\mathbf{z} \in \mathbb{H}^d$;

Output: $\omega \in \mathbb{H}_p^d$;

- 1: Split the full quaternionic array \mathbf{z} to a real matrix $\mathbf{M} \in \mathbb{R}^{d \times 4}$.
- 2: Compute the eigenvalue and eigenvector of $\mathbf{W} = \mathbf{M}^T \mathbf{M}$ which is a 4×4 matrix, obtain the eigenvector \mathbf{v} of \mathbf{W} corresponding to its smallest eigenvalue.
- 3: Let $q = v_1 + v_2i + v_3j + v_4k$ be the phase factor and obtain its quaternionic conjugation $\bar{q} = v_1 - v_2i - v_3j - v_4k$.
- 4: **for all** $i = 0, 1, \dots, T - 1$ **do**
- 5: Compute the left product of \mathbf{z} by \bar{q} , i.e.

$$\mathbf{p} = \mathbf{z} \cdot \bar{q}.$$

- 6: Let ω be the imaginary part of \mathbf{p} .
 - 7: **end for**
 - 8: **return** $\omega \in \mathbb{H}_p^d$.
-

At the end of this section, we provide a combination of QPFE and QRAF for pure quaternion signals, referred to as PQRAF. Combinations with other algorithms used in the Section 7 can be formulated similarly.

Algorithm 8 Pure Quaternionic Reweighted Amplitude Flow (PQRAF)

Input: Data $(\alpha_k, \psi_k = |\alpha_k^* \mathbf{x}|)_{k=1}^n$, step size η , weighting parameters β , subset cardinality $|\mathcal{S}|$, exponent γ and the iteration number T . Moreover, the step parameter T_p ;

Output: \mathbf{z}_T ;

- 1: Initialization as in Algorithm (1) to obtain $\mathbf{z}_0 = \lambda_0 \cdot \mathbf{v}_{in}$.
 - 2: **for all** $i = 0, 1, \dots, T - 1$ **do**
 - 3: Compute $\nabla \ell_{\text{rw}}(\mathbf{z}_i)$ and update \mathbf{z}_{i+1} as in Algorithm 1.
 - 4: **if** $\text{mod}(i, T_p) = 0$ **then**
 - 5: Compute $\omega_{i+1} \in \mathbb{H}_p^d$ by calling QPFE as in Algorithm 7 with the input \mathbf{z}_{i+1} .
 - 6: Update $\mathbf{z}_{i+1} = \omega_{i+1}$.
 - 7: **end if**
 - 8: **end for**
 - 9: **return** \mathbf{z}_T .
-

Similar to [9], we use T_p to be the parameter that controls the transform of full

quaternion to pure quaternion signals. Unlike [9] which utilizes inner and outer loop for the result, we only perform QPFE once after T_p iteration periodically. In our algorithm, the total iteration number is the given parameter T compare to the actual iteration number $T \times T_p$ in [9].

It is easily to see that the parameter T_p makes difference when it changes, especially when $T_p = 1$ which means operate QPFE in every iteration and $T_p = T$ which means operate QPFE at the final step of the full quaternion algorithm. Although there are difference among them, the actual computation shows no essential distinction. Since our work considers mainly on different algorithms rather than different aspects of a single algorithm, we prefer to save this part of work in the future.

7. Numerical Experiments

In this section, we show the numerical efficiency of QRAF and its improvements by comparing their the performance with other competitive methods. Specifically, Section 7.1 is for synthetic data, while Section 7.2 focuses on color image processing. Additionally, Section 7.3 provides a comparative analysis of conventional and quaternion-based algorithms.

Table 1: Parameters in algorithms

Algorithm	Parameters
QWF	$\eta = \frac{0.2n}{\sum_{k=1}^n y_k}$;
QRWF	$\alpha_\ell = 1, \alpha_u = 5$ and $\mu = 0.8$;
QPAF	$\gamma = 1/2, \eta = 2.5$ and $\sigma = 2$;
QTAF	$\gamma = 0.8, \eta = 1.2$ and $\rho = \frac{1}{6}$;
QRAF	$ \mathcal{S} = \lfloor 3n/13 \rfloor, \beta = 5, \gamma = 0.5$ and $\mu = 6$;
QARAF	$\eta = 6$ and $\mu = 0.8$;
QAdRAF	$\alpha = 0.009, \mu = 1, \epsilon = 10^{-6}$;
QIRAF	$\eta = 6$ and batch size $ \Gamma = 2^k, k = \frac{\log(\frac{n}{4}-1)}{\log 2}$.

Throughout our work, the parameters of the tested algorithms are listed in Table 1. For the existing quaternionic algorithm QWF, we use the given parameters there. For the algorithms that transferred from the real or complex space, we compare the original parameters with a huge a mount of tested parameters to obtain a suitable set of parameters.

7.1. Synthetic Data

This subsection presents a performance comparison of various quaternionic algorithms, evaluated through experimental results. In each trial, we employ a Gaussian measurement ensemble $\mathbf{A} \sim \mathcal{N}_{\mathbb{H}^{n \times d}}$. The entries of quaternion signal $\mathbf{x} \in \mathbb{H}^d$ are independent and identically distributed (i.i.d.) as $\mathcal{N}(0, 1) + \sum_{v=i,j,k} \mathcal{N}(0, 1)v$. The signal \mathbf{x} is subsequently normalized to satisfy $\|\mathbf{x}\| = 1$. Note that to approximate the leading eigenvector of the Hermitian matrix, we perform 100 power iterations. The power method (see e.g., [30]) used for quaternion Hermitian matrix is analogous to the approach used in the complex case.

i. Convergence performance Firstly, we examine the convergence of each algorithm, as shown in Fig. 1 and Fig. 2. The relative error, defined as $\text{dist}(x, z)/\|x\|$ and $\text{dist}_p(x, z)/\|x\|$ w.r.t full and pure quaternion algorithms respectively, serves as the convergence criterion. It is seen that all algorithms are convergent albeit at different rates. The convergence rate is a crucial aspect and is influenced not only by the algorithm’s gradient but also by other factors, such as the vector dimension d , the ratio n/d , and the algorithm’s initialization.

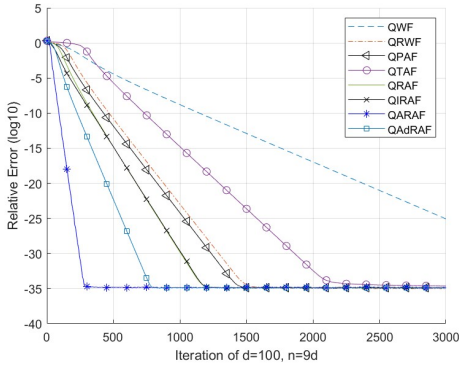


Figure 1: Simulations of different algorithms on quaternion-valued signals

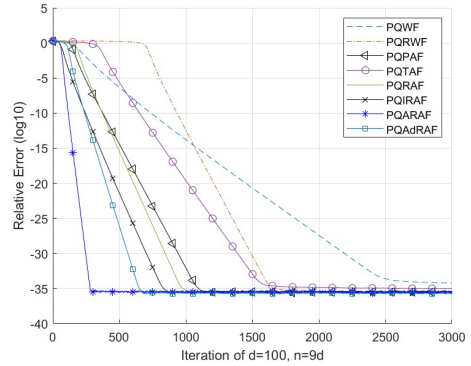


Figure 2: Simulations of different algorithms on signals of pure quaternions

In this sample, we set $n/d = 9$ to simply investigate its convergence. It is easy to see that in general all algorithms converge to the same level of relative error, i.e. $\ln(10^{-35})$, but there are some details that must be noted.

For the full quaternion algorithms in Fig. 1, QARAF leads the competition of convergence with the iteration number less than 400. QRAF and its variants converge evidently faster than other algorithms. The QWF also converges but with a lower speed that is not fully shown in the figure. We should note that the curves of QRAF and QIRAF almost cover each other, showing the same ability of convergence. This is actually important since

as the variants of QRAF, QIRAF has the advantage of computation speed which we will discuss later in details.

Similar to the full quaternion algorithms, the pure ones have the same level and order of convergence. Note that with the assist of QPFE, the gradients vary on certain area, depending on the merit of algorithms themselves. But in general, the full quaternion algorithms and the pure ones admit the same level of performance.

ii. Success rate Next, we report the success rates of the QRAF, QRWF, QTAF, QWF and QIRWF algorithms under different sample size. Specifically, for a vector $\mathbf{x} \in \mathbb{H}^d$ with $d = 100$, we conduct 100 trials for each value of n/d , ranging from 3 to 13 in increments of 0.5. Taking into account $5 < n/d < 8$ is critical, the step size was reduced to 0.2 to provide clear insights in the corresponding figure. Each algorithm was run for 1500 iterations per trial. Similar as [9, 17], a trial was deemed successful if it achieved $\text{dist}(\mathbf{x}, \mathbf{z}) < 10^{-5}$ within the 1500 iterations. The parameters used for each algorithm are listed in the Table 1, and the success rate regarding to n/d is in Fig. 3 and Fig. 4.

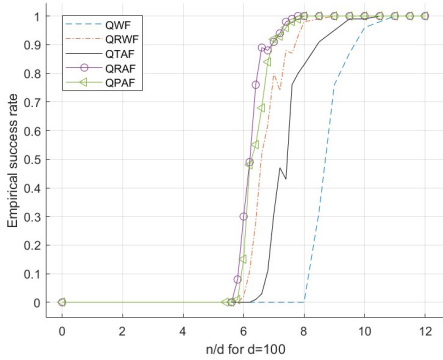


Figure 3: Success rate of different quaternion algorithms

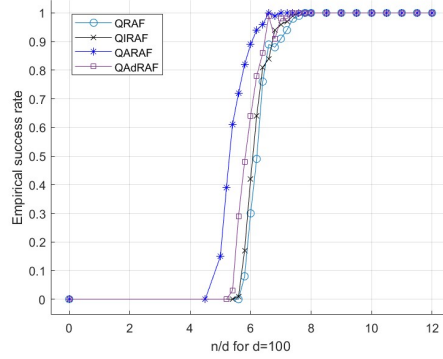


Figure 4: Success rate of QRAF and its variants

In order to show results in detail, we split the algorithms in two sets, i.e. in Fig. 3 and Fig. 4. For the comparison of Wirtinger flow (QWF, QRWF) and Amplitude flow (QTAF, QRAF, QPAF), it can be easily seen that QRAF performs an overall advantage in success rate than other algorithms. Meanwhile, QPAF performs also well in this index with a success rate equals to 1 when n/d equals to 8. This value is larger than 10 in algorithms such as QWF and QTAF. Since n/d rate is decisive in computation cost, for the same success rate, a lower n/d value means less computation, higher speed and less computer memory requirement. Thus in this point of view, QRAF outperform other algorithms in this set.

However, in the set of QRAF and its variants in Fig. 4, there is another story. The most

attention-tracking algorithm is QARAF which reduces the n/d rate to 7 to get the success rate of 1 and outperformed other algorithms. This algorithm enjoys an accelerated steepest decent method as introduced in subsection 4.2. The QAdRAF with an adapted gradient decent method also performed better than QRAF, thus better than other algorithms in the previous set in Fig. 3. Critically, the QIRAF seems no difference with QRAF which is the important. With the mini-batch strategy, QIRAF decrease huge amount of computation but loose almost nothing in success rate. This enables QIRAF performed as fast (see Table 2) as QARAF which plays an important role in in practical.

It worth mention two things in this index (success rate). Firstly, since we define a success as the algorithm achieves $\text{dist}(\mathbf{x}, \mathbf{z}) < 10^{-5}$ within 1500 iterations, for a single trial, one can not tell whether the algorithm achieves this threshold after 100 iterations or 1400 iterations. Secondly, there are points of inflection on the curve, showing the oscillation of success rate. The main reason is that the measurement matrix is drawn with randomness and n/d rates are very close (merely 0.2) among the points of inflection. It is easy to understand that if we increase the step size in n/d rate or run more trials, the inflection points will disappear. But both remarks show that the index of success rate is more of a general comparison of algorithms rather than detailed evaluation. Thus the step size and the trial amount that we have chosen is enough for the study.

Although the **oversampling rate** n/d is crucial in Phase Retrieval, it is not the only factor that matters. The length of the original signal d also plays an important role in algorithm performance, in this case the success rate. To further explore this, we conducted additional trials on QRAF and its variants with varying dimensions, setting $d = 30 : 30 : 300$ and $n/d = 3 : 0.5 : 10$. For each parameter pair $(d, n/d)$, 30 trials were conducted to calculate the success rate, i.e. achieve $\text{dist}(x, z) < 10^{-5}$ within 1500 iterations. Notably, when $d = 100$, the slices of the following figures align with the curves in Fig. 4 respect to the corresponding algorithm.

From above figures, we can easily seen that the signal dimension also affect tested algorithms on convergence at some level. For instance, when $d = 30$ and $n/d = 6$, the success rate of QIRAF is 0.83 while when $d = 300$ the success rate is 0 with the same n/d . Another example is when $d = 60$ and $n/d = 6.5$ the success rate is 1, but when $d = 300$ and $n/d = 6.5$, the success rate is 0.33. (The original data is uploaded and can be verified by any means.)

In another word, as d increases, the ratio n/d must also be larger to achieve a high success rate. It is worth noting that, compared to QRAF algorithm, the QIRAF is more sensible to the size of vector $\mathbf{x} \in \mathbb{H}^d$. And the QARAF is the most stable one, comparing to its counterparts.

iii. Compete test for quaternionic algorithms Table 2 provides an overview of the features of different algorithms. For these experiments, the parameters were set according

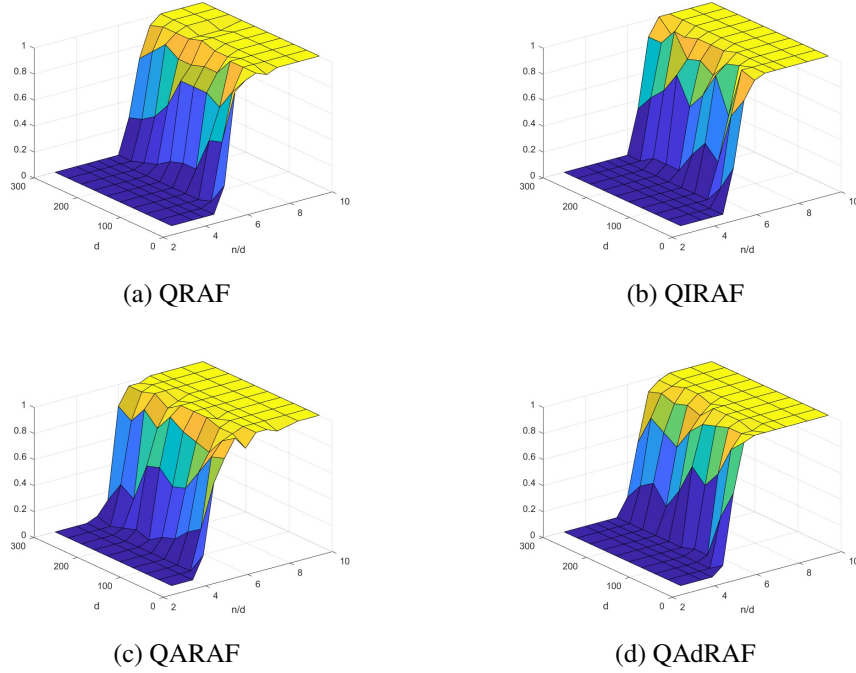


Figure 5: Success rate of QRAF and its variants in various views

to Table 1 and set $n/d = 9$, with $d = 64$ and $d = 100$ separately. Each algorithm was run for 100 trials with the results averaged. It should be noted that for algorithms that success rate did not reach 1, the average convergence time and iterations exclude the cases of non-converging.

Table 2: Comparison of iteration count and time cost among quaternionic algorithms

Algorithm:	d	QWF	QRWF	QPAF	QTAF	QRAF	QIRAF	QARAF	QAdRAF
Success rate:		0.81	0.99	1	1	1	1	1	1
Iterations:	64	1280.12	518.84	457.04	734.08	378.86	382.50	100.99	249.44
Time (s):		93.52	34.82	29.23	52.54	27.45	11.32	7.01	16.32
Success rate:		0.74	1	1	0.96	1	1	1	1
Iterations:	100	1326.47	594.07	501.27	824.76	409.63	389.74	106.85	272.92
Time (s):		244.97	101.16	86.10	140.12	68.02	19.11	18.86	48.59

The performance of quaternionic Wirtinger Flow and quaternionic Amplitude Flow algorithms are exhibited in Table 2. Consider together with Fig. 3 and Fig. 4 when $d = 100$, it is easily seen that QRAF and its variants surpasses other kinds algorithms in

this table not only in success rate but also in convergence step and time consumption. This overall advantage is evident in both cases of $d = 64$ and $d = 100$.

When it comes to QRAF and its variants themselves, the competition becomes much intenser, but QARAF wins without doubts. All QRAF-type algorithms have a success rate of 1 but QARAF has lower convergence step number and less time consumption by the acceleration technique. Note that QARAF is less influenced by the size of the signal, from 100.99 to 106.85 as d increases from 64 to 100, comparing to other algorithms. This also aligns the conclusion of Fig. 5.

Another outstanding algorithm is QIRAF, which must be studied carefully. Consider Table 2 and Fig. 1 and Fig. 4 together, we can easily observe that the performance of QIRAF and QRAF are much similar. However, QIRAF enjoys much less computation than QRAF by the mini-batch technique without losing much advantage of gradient. This is an essential virtue in practical.

Meanwhile, though QIRAF does not outperform QARAF when d equals to 64 or 100 in both iteration count and time consumption, it can not be simply deemed as a complete fail to the latter. While QARAF gets the result of less time consumption by less convergence step, QIRAF achieved the same level of less time consumption by less computation. In another word, the average time per step of QIRAF is less than QARAF. Therefore, when d gets larger (for instance when $d > 200$), QIRAF will use less time than QARAF in the same task while success rate still be 1.

One more thing needs to be mentioned is that, QARAF having such an outstanding performance comes with a cost of algorithm complexity and CPU memory. Although the cost is not expensive enough to be considered essential, it can be clearly noticed in practical in time-consumption per iteration step. This is actually the secondary factor that QARAF and QIRAF have competition in time consumption, while QARAF is far beyond QIRAF in convergence step. Algorithm performance is always about the balance of time consumption, computation and machine memory.

7.2. Experiment: Color Images

In this section, we compare different quaternionic algorithms in processing real images. The images used for testing are sourced from the Kodak dataset¹, i.e. 4.1.04 (256×256), 4.1.05 (512×512) and 4.2.03 (256×256).

Ideally, the entire image would be considered as the signal for reconstruction. However, due to computational limitations present not only in quaternionic algorithms but also in real and complex algorithms, we adopt the conventional approach of segmenting each image into smaller blocks and treating each block as a separate signal \mathbf{x} to be reconstructed.

¹<https://www.kaggle.com/datasets/sherylmehta/kodak-dataset>

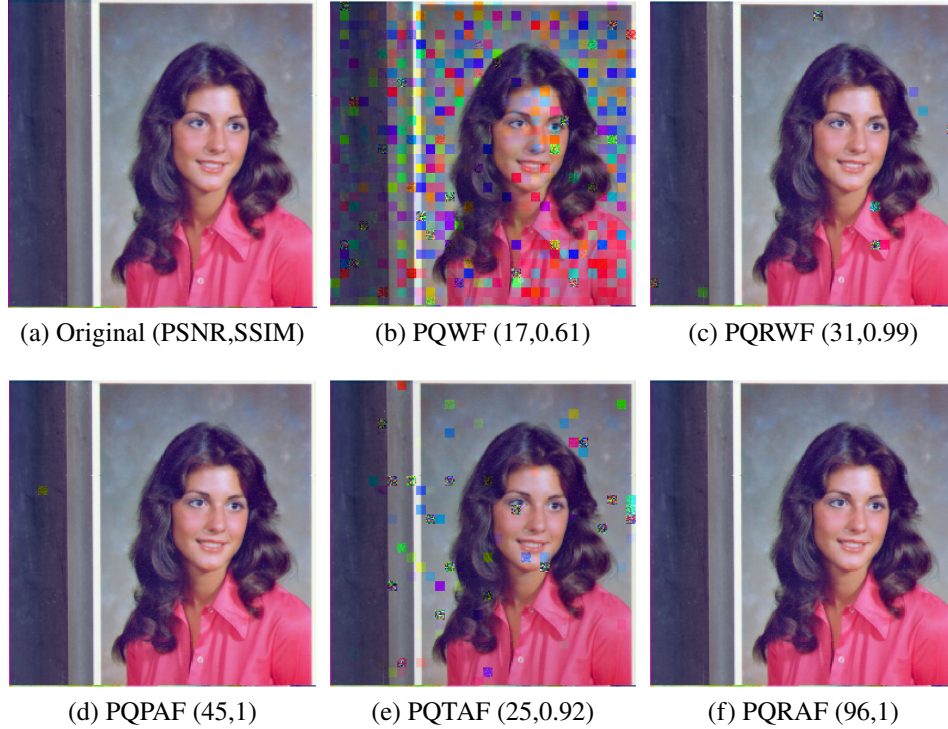


Figure 6: Comparison of PQWFs and PQAFs

Specifically, in the first experiment, i.e. Fig. 6, we test the picture 4.1.04 in Kodak dataset as in [9]. The picture is 256×256 , we split this picture into 32×32 pieces, then each piece is a 8×8 block containing 64 pixel which is the signal \mathbf{x} and its size $d = 64$. In the second experiment, i.e. Fig. 7, the figure 4.1.05 of the size 512×512 is also tested. The figure is divided also into 32×32 pieces but with each block of 16×16 pixels. Therefore, in this experiment, the size of the signal \mathbf{x} is $d = 256$.

For these experiments, we set the n/d ratio to 9 and fixed the total number of iterations to $T = 300$ for each algorithm. The outcomes are presented in Fig. 6.

The results in Fig. 6 clearly highlight the performance of each algorithm. In comparison with the original image, only the reconstruction by PQRAF (see Fig. 6f) contains no defective blocks, indicating the robustness of this algorithm. PQPAF and PQRWF also perform well, with only a few defective blocks, reflecting the varying strengths of WF and AF. Conversely, PQWF and PQTAF exhibit relatively weaker performance, illustrating that different WF and AF algorithms have trade-offs in terms of convergence speed and overall effectiveness.

To quantify these observations, we utilize two evaluation metrics: Peak Signal-to-

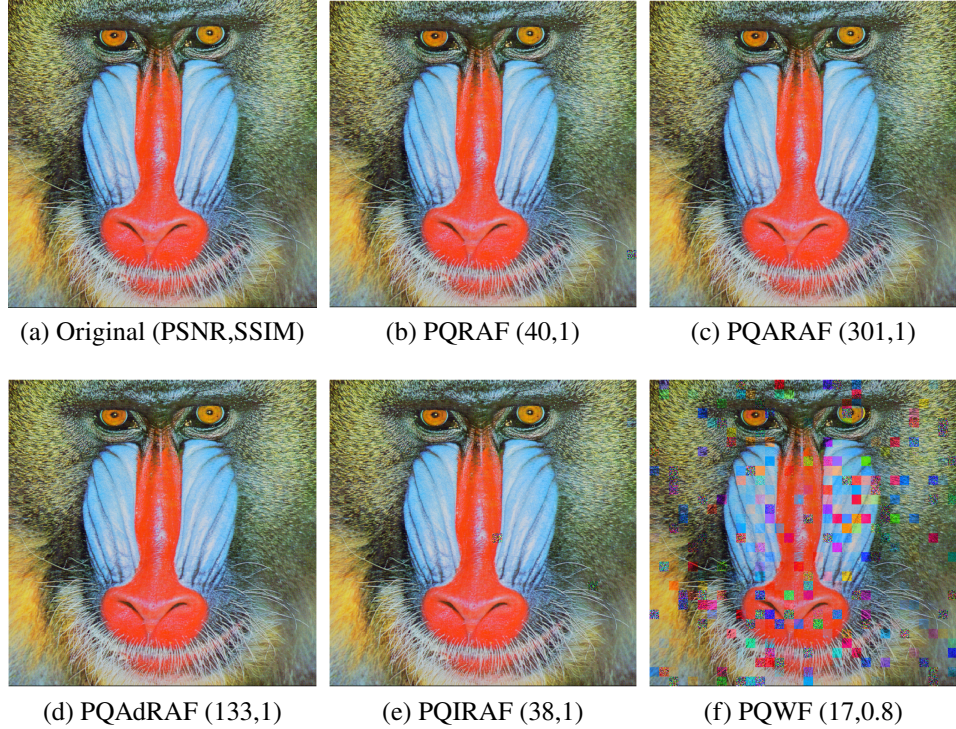


Figure 7: Comparison of the variations of QRAF

Noise Ratio (PSNR) and Structural Similarity Index Measure (SSIM). PSNR measures the similarity between the original and reconstructed images, with higher values indicating closer similarity. SSIM assesses structural similarity, ranging from 0 to 1, where a score of 1 denotes perfect similarity.

The indices reveal that PQRAF significantly outperforms other algorithms, achieving the highest PSNR score of 96 in this experiment. Additionally, both PQRAF and PQPAF attain the maximum SSIM score of 1, leading the competition in this aspect. These indices corroborate the earlier qualitative observations with a more precise, quantitative evaluation.

In the subsequent experiment, we operate algorithms of QRAF and its variants, namely, PQARAF, PQAdRAF and PQIRAF to compare their performance (PQWF as control group). The setting of this experiment is aforementioned and the results are displayed in Fig. 7. It is noteworthy that the QRAF-based algorithms share the same initialization method, therefore gradients are the only difference among these algorithms.

Compared to the previous experiment, QRAF and its variants all exhibit exceptional performance, successfully reconstructing the signals without any defective blocks. While visual inspection may not easily reveal differences among these results, the quantitative

indices provide a more reliable assessment. In this experiment, SSIM loses its discriminatory power, as all algorithms achieve a score of 1, reflecting their high accuracy. However, PQARAF stands out with a significantly higher PSNR of 301, surpassing other variants. Meanwhile, the performance of PQRAF and PQIRAF in terms of PSNR remains very close, showing the same ability of reconstructing signals in practical.

7.3. Comparison of conventional and quaternionic algorithms

It is *natural* and *frequently* to question the advantage of the Phase Retrieval in the quaternionic approach. While the problem can indeed be addressed in both the real and quaternionic domains, the quaternionic approach offers more than just an alternative method; it also provides certain practical benefits that enhance the research field. To illustrate this, we compare the Quaternionic Reweighted Amplitude Flow (QRAF) to the real Reweighted Amplitude Flow (RAF) algorithms.

Similar to [9], we slightly modify the structure of the given quaternion signal to fit the real RAF algorithms. Here we propose two forms of real RAF algorithms, i.e., **RAF of a monochromatic model** (denoted by RAF-Mono) and **RAF of a concatenation model** (denoted by RAF-Conc).

For a pure quaternion signal $\mathbf{p} \in \mathbb{H}_p^d$, the RAF of a monochromatic model separately reconstruct $\mathcal{P}^i(\mathbf{p})$, $\mathcal{P}^j(\mathbf{p})$ and $\mathcal{P}^k(\mathbf{p})$, which are three real signal in \mathbb{R}^d . We denote by $\hat{\mathbf{z}}^i$, $\hat{\mathbf{z}}^j$ and $\hat{\mathbf{z}}^k$ the reconstructed signal corresponding to each channel. To keep the metric consistent, the reconstruction error for real RAF of a quaternion signal \mathbf{p} is measured as $\left(\sum_{h=i,j,k} \text{dist}_p(\mathcal{P}^h(\mathbf{p}), \hat{\mathbf{z}}^h)^2\right)^{1/2}$.

On the other hand, the concatenation model of real RAF for a pure quaternion signal $\mathbf{p} \in \mathbb{H}_p^d$ also split the signal as $\mathcal{P}^i(\mathbf{p})$, $\mathcal{P}^j(\mathbf{p})$ and $\mathcal{P}^k(\mathbf{p})$, and concatenate the three real vector into a new signal, i.e. $\hat{\mathbf{p}} = \left[(\mathcal{P}^i(\mathbf{p}))^T, (\mathcal{P}^j(\mathbf{p}))^T, (\mathcal{P}^k(\mathbf{p}))^T \right]^T \in \mathbb{R}^{3d}$. We denote by $\hat{\mathbf{z}} \in \mathbb{R}^{3d}$ the reconstructed signal, then the measurement for reconstruction error of this algorithm is defined as $\text{dist}_p(\hat{\mathbf{p}}, \hat{\mathbf{z}})$.

i. Compete test in convergence and success rate Firstly, we investigate the performance of algorithms in convergence and success rate as before. To compare with RAF-Mono and RAF-Conc, we test pure quaternionic algorithms, since the given signal here is pure quaternion $\mathbf{p} \in \mathbb{H}_p^d$.

It can be easily seen from Fig. 8 that quaternionic algorithms converge faster than real algorithms, which PQARAF reach the relative error of $\ln(10^{-35})$ within 500 iterations. From Fig. 9, we can observe that PQRAF and its variants have much lower n/d rate to achieve the success rate of 1 in this experiment.

However, one advantage of real algorithms that quaternionic ones cannot have is the time consumption. From Table 3, we can easily observe that, though PQRAF and its

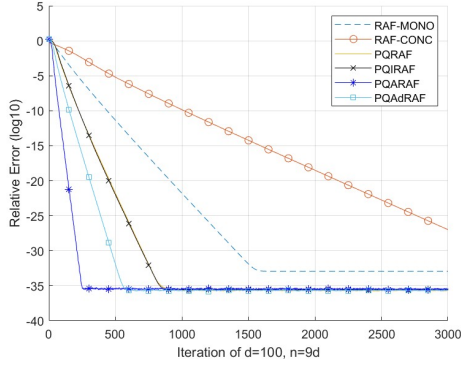


Figure 8: Convergence of real and pure quaternion algorithms

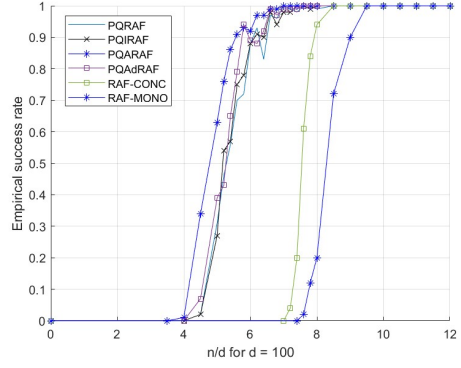


Figure 9: Success rate of real and pure quaternion algorithms

Table 3: Comparison of iteration count and time cost among algorithms

Algorithm:	d	PQRAF	PQIRAF	PQARAF	PQAdRAF	RAF-MONO	RAF-CONC
Success rate:		1	1	1	1	1	1
Iterations:	64	281.12	278.74	84.95	192.08	487.78	1149.13
Time (s):		20.65	8.12	6.37	13.58	2.69	3.21
Success rate:		1	1	1	1	1	1
Iterations:	100	299.54	288.64	93.52	211.16	484.43	1160.02
Time (s):		52.89	15.22	16.47	37.30	4.39	4.96

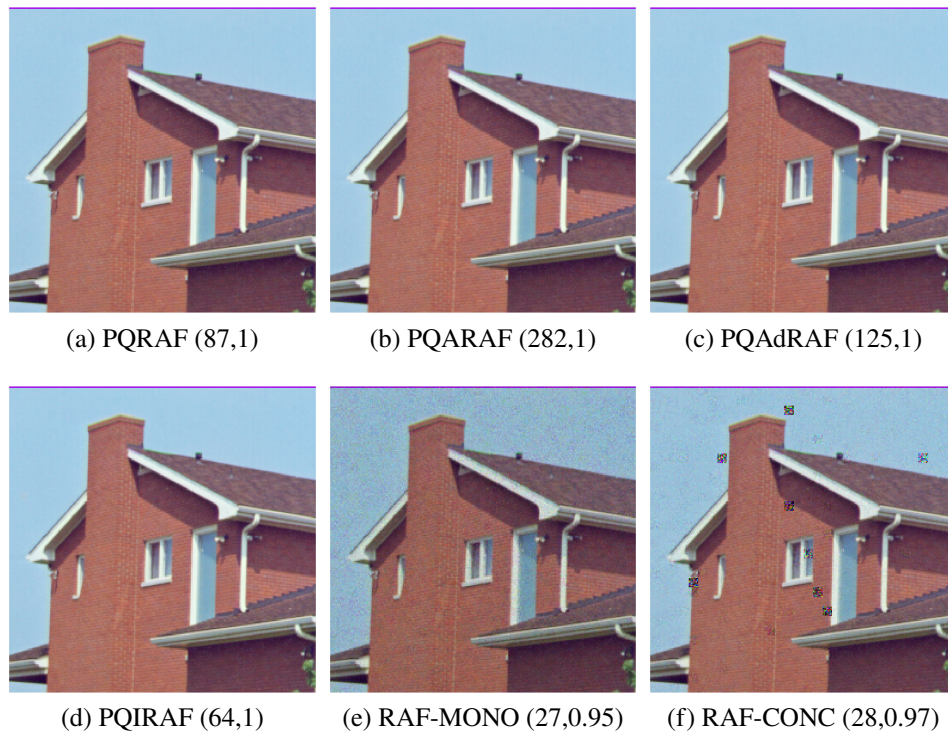


Figure 10: Comparison of quaternionic and real algorithms

variants have much less average convergence steps, they cannot compete with RAF-Mono and RAF-Conc in time consumption.

The only reason of this situation is that we use MATLAB to run the experiments, which is a professional software to deal with matrix computation especially in real and complex field, thus for RAF-Mono and RAF-Conc, it is suitable for these algorithm. There are no such a special software for quaternion algorithms at present. Much of the time consumption is used on quaternion-to-real and quaternion-to-complex matrix transformation to complete the computation.

ii. Comparison of quaternionic and real algorithms in color image In this section, we compare real PR algorithms and the quaternionic ones in reconstructing color images. The image to be tested is 4.1.05 from the data set. The size of the image is 256×256 . Similar to the first experiment in Fig. 6, we split the image into 32×32 piece with each piece is of 8×8 pixels. The total iteration is still 300 and we set n/d rate to 9 as always. The results is shown in Fig. 10.

From the result, it is evident that PQRAF and its variants achieve superior results with the same number of iterations compared to real RAF algorithms. After the same number

of iterations, RAF-Conc still displays some defective blocks, and RAF-Mono appears generally darker than the original image. In contrast, all quaternionic algorithms produce well-reconstructed images without any noticeable defects.

These differences can be quantitatively assessed using indices similar to those employed in the experiment depicted in Fig. 6. Specifically, PQARAF significantly outperforms other algorithms, achieving a PSNR of 282 and an SSIM of 1. In comparison, the real algorithms RAF-Mono and RAF-Conc attain PSNR values of 27 and 28, and SSIM scores of 0.95 and 0.97, respectively. The relatively lower PSNR and non-optimal SSIM values for the real algorithms indicate their inferior performance relative to the quaternionic algorithms.

However, one thing that cannot be neglected is that real RAF algorithms are evidently faster than quaternionic ones in reconstructing a image as we already mentioned. By simply increasing the n/d rate without any time consumption piles up, real algorithms can surpass the quaternionic ones in convergence as well. However, such comparisons would no longer adhere to the same standard, and thus fall outside the scope of this study.

8. Conclusion

In this paper, we address the quaternionic phase retrieval problem by systematically developing the Quaternionic Reweighted Amplitude Flow (QRAF) algorithm based on an amplitude-based model. The QRAF is further improved by three distinct variants. Numerical results, using both synthetic data and real images, show that our algorithms substantially improve recovery performance and computational efficiency compared to state-of-the-art approaches.

One limitation of QRAF is the absence of a proof for the LCR condition as present in Problem 3.5. This challenge is not unique to the quaternionic domain but also persists in the complex domain. We believe that once the LCR condition is established for complex signals, the proof can be extended to the quaternionic setting without substantial difficulty. Alternatively, to address the difficulty, we considered a perturbed amplitude-based model and developed a non-convex QPAF algorithm. QPAF exhibits comparable performance to QRAF while has theoretical guarantee of linear convergence, which can be extended from proof for complex case.

Furthermore, it is important to note that while quaternionic algorithms offer clear advantages in terms of convergence steps and success rate, their drawback in terms of computational time compared to real-valued algorithms cannot be overlooked. The current implementation of quaternionic algorithms relies on matrix computation techniques. Although the execution speed of these implementations may not be as competitive as real-valued algorithms—largely due to optimizations like MATLAB’s highly accelerated

matrix operations—this does not impact the computational complexity or the fundamental priorities of the algorithms under these conditions.

Acknowledgments

This work was partially supported by NSFC Grant No.12101451.

References

- [1] S. Miron, J. Flamant, N. Le Bihan, P. Chainais, D. Brie. Quaternions in signal and image processing: A comprehensive and objective overview. *IEEE Signal Process. Mag.* **40** (2023), 26–40.
- [2] R. Jacome, K. V. Mishra, B. M. Sadler, et al. An invitation to hypercomplex phase retrieval: Theory and applications. *IEEE Signal Process. Mag.* **41** (2024), 22–32.
- [3] T. A. Ell, N. Le Bihan, S. J. Sangwine. Quaternion Fourier transforms for signal and image processing. *John Wiley & Sons*, 2014.
- [4] R. Jacome, K. V. Mishra, B. M. Sadler, et al. Octonion phase retrieval. *IEEE Signal Process. Lett.* **31** (2024), 1615–1619.
- [5] M. Zimmermann, S. Bernstein, B. Heise. Quaternionic phase and axis/colour retrieval. *Signal Image Video Process.* **17** (2023), 3865–3871.
- [6] H. De Bie. Clifford algebras, Fourier transforms, and quantum mechanics. *Math. Meth. Appl. Sci.* **35** (2012), 2198–2228.
- [7] E. Hitzler. Quaternion and Clifford Fourier transforms. Chapman and Hall/CRC, New York, 2021.
- [8] G. Wang, B. Giannakis, C. Eldar. Solving systems of random quadratic equations via truncated amplitude flow. *IEEE Trans. Inf. Theory.* **64** (2024), 773–794.
- [9] J. Chen, M. Ng. Phase retrieval of quaternion signal via Wirtinger flow. *IEEE Trans. Signal Process.* **71** (2023), 2863–2878.
- [10] M. Hobiger, N. Le Bihan, C. Cornou, P. Bard. Multicomponent signal processing for Rayleigh wave ellipticity estimation: Application to seismic hazard assessment. *IEEE Signal Process. Mag.* **29** (2012), 29–39.

- [11] C. Took, D. Mandic. The Quaternion LMS algorithm for adaptive filtering of Hyper-complex processes. *IEEE Trans. Signal Process.* **57** (2009), 1316–1327.
- [12] C. Zou, K. I. Kou, Y. Wang. Quaternion collaborative and sparse representation with application to color face recognition. *IEEE Trans. Image Process.* **25** (2016), 3287–3302.
- [13] T. Parcollet, M. Morchid, G. Linaresg. A survey of quaternion neural networks. *Artificial Intelligence Review.* **53** (2020), 2957–2982.
- [14] L. Taylor. The phase retrieval problem. *IEEE Trans. Antennas Propag.* **29** (1981), 386–391.
- [15] Y. Shechtman, Y. C. Eldar, O. Cohen, at el. Phase retrieval with application to optical imaging: A contemporary overview. *IEEE Signal Process. Mag.* **32** (2015), 87–109.
- [16] H. Zhang, Y. Zhou, Y. Liang, at el. A nonconvex approach for phase retrieval: reshaped Wirtinger flow and incremental algorithms. *J. Mach. Learn. Res.* **18** (2017), 1–35.
- [17] G. Wang, B. Giannakis, Y. Saad, J. Chen. Phase retrieval via reweighted amplitude flow. *IEEE Trans. Signal Process.* **66** (2018), 2818–2833.
- [18] E. J. Candès, T. Strohmer, V. Voroninski. Phaselift: exact and stable signal recovery from magnitude measurements via convex programming. *Commu. Pure. Appl. Math.* **66** (2013), 1241–1274.
- [19] E. J. Candès, Y. C. Eldar, T. Strohmer, V. Voroninski. Phase retrieval via matrix completion. *SIAM Review.* **57** (2015), 225–251.
- [20] E. J. Candès, X. Li, M. Soltanolkotabi. Phase retrieval via Wirtinger flow: theory and algorithms. *IEEE Trans. Inf. Theory.* **61** (2015), 1985–2007.
- [21] Y. Chen, E. Candès. Solving random quadratic systems of equations is nearly as easy as solving linear systems. *Commun. Pure Appl. Math.* **70** (2017), 822–883.
- [22] S. Lazendić, H. De Bie, A. Pižurica. Octonion sparse representation for color and multispectral image processing. *European Signal Processing Conference.* 2018, 608–612.
- [23] Y. Chen, C. Cheng, Q. Sun. Phase retrieval of complex and vector valued functions. *J. Funct. Anal.* **283** (2022), 109593.

- [24] F. Zhang. Quaternions and matrices of quaternions. *Linear Algebra Its Appl.* **251** (1997), 21–57.
- [25] D. Xu, D. Mandic. The theory of quaternion matrix derivatives. *IEEE Trans. Signal Process.* **63** (2015), 1543–1556.
- [26] P. Netrapalli, P. Jain, S. Sanghavi. Phase retrieval using alternating minimization. *Advances in Neural Information Processing Systems (NIPS)* 2013.
- [27] R. Kolte, A. Özgür. Phase retrieval via incremental truncated Wirtinger flow. arXiv:1606.03196, 2016.
- [28] H. Xiong, Y. Chi, B. Hu, et al. Convergence analysis of accelerated first-order methods for phase retrieval. *23rd International Symposium on Mathematical Theory of Networks and Systems Hong Kong University of Science and Technology, Hong Kong, July 16-20, 2018.*
- [29] Y. Qin. Phase retrieval via accelerated gradient descent. *Artificial Intelligence and Security: 5th International Conference, ICAIS 2019, New York, NY, USA, July 26–28, 2019, Proceedings, Part III 5.* Springer International Publishing, 2019, 47–55.
- [30] Y. Li, M. Wei, F. Zhang, J. Zhao. On the power method for quaternion right eigenvalue problem. *J. Comput. Appl. Math.* **345** (2019), 59–69.
- [31] J. Sun, Q. Qu, J. Wriqh. A geometric analysis of phase retrieval. *Found. Comput. Math.* **18** (2018), 1131–1198.
- [32] R. Delanghe, F. Sommen, V. Souček. *Clifford Algebra and Spinor-Valued Functions*, vol. 53 of Mathematics and its Applications. Kluwer Academic Publishers Group: Dordrecht, 1992.
- [33] B. Gao, X. Sun, Y. Wang, et al. Perturbed amplitude flow for phase retrieval. *IEEE Trans. Signal Process.* **68** (2020), 5427–5440.
- [34] A. Badeńska, Ł. Błaszczyk. Quaternion Gaussian matrices satisfy the RIP. arXiv:1704.08894, 2017.
- [35] Y. Chen, X. Xiao, Y. Zhou. Low-rank quaternion approximation for color image processing. *IEEE Trans. Image Process.* **29** (2020), 1426–1439.